AGU PUBLICATIONS

JGR

Journal of Geophysical Research: Biogeosciences

RESEARCH ARTICLE
10.1002/2017JG004279

Key Points:
- The FRE biomass combustion coefficient (FBCC) that relates satellite FRE to biomass consumption was examined over 455 wildfire events
- The results confirm the linearity of the empirical relationship between satellite FRE and the total biomass consumption for wildfires
- The derived FBCC was 0.374 kg/MJ for GOES FRE, 0.266 kg/MJ for MODIS FRE, and 0.320 kg/MJ considering the average GOES and MODIS FRE

Correspondence to:
X. Zhang,
xiaoyang.zhang@sdstate.edu

Citation:
Li, F., Zhang, X., Kondragunta, S., & Roy, D. P. (2018). Investigation of the fire radiative energy biomass combustion coefficient: A comparison of polar and geostationary satellite retrievals over the Conterminous United States. *Journal of Geophysical Research: Biogeosciences*, *123*, 722–739. https://doi.org/10.1002/2017JG004279

Received 2 NOV 2017
Accepted 13 FEB 2018
Accepted article online 20 FEB 2018
Published online 28 FEB 2018

Investigation of the Fire Radiative Energy Biomass Combustion Coefficient: A Comparison of Polar and Geostationary Satellite Retrievals Over the Conterminous United States

Fangjun Li[1], Xiaoyang Zhang[1], Shobha Kondragunta[2], and David P. Roy[1]

[1]Geospatial Sciences Center of Excellence, South Dakota State University, Brookings, SD, USA, [2]Center for Satellite Applications and Research, NESDIS, NOAA, College Park, MD, USA

Abstract Biomass burning substantially contributes to atmospheric aerosol and greenhouse gas emissions that influence climate and air quality. Fire radiative energy (FRE) (units: MJ) has been demonstrated to be linearly related to biomass consumption (units: kg) with potential for improving biomass burning emission estimation. The scalar constant, termed herein as the FRE biomass combustion coefficient (FBCC) (units: kg/MJ), which converts FRE to biomass consumption, has been estimated using field and laboratory experiments, varying from 0.368 to 0.453 kg/MJ. However, quite different FBCC values, especially for satellite-based approaches, have been reported. This study investigated the FBCC with respect to 445 wildfires that occurred from 2011 to 2012 across the Conterminous United States (CONUS) considering both polar-orbiting and geostationary satellite data. The FBCC was derived by comparing satellite FRE estimates with biomass consumption for the CONUS. FRE was estimated using observations from the Moderate Resolution Imaging Spectroradiometer (MODIS) and the Geostationary Operational Environmental Satellite (GOES); biomass consumption was estimated using Landsat-derived burned areas with fuel loadings from the Fuel Characteristic Classification System and using combustion completeness parameterized by Landsat burn severity and Fuel Characteristic Classification System fuelbed type. The reported results confirm the linearity of the empirical relationship between FRE and biomass consumption for wildfires. The CONUS FBCC was 0.374 kg/MJ for GOES FRE, 0.266 kg/MJ for MODIS FRE, and 0.320 kg/MJ considering both GOES and MODIS FRE. Limited sensitivity analyses, comparing MODIS and GOES FRE with biomass consumption estimated in three different ways, indicated that the FBCC varied from 0.301 to 0.458 kg/MJ.

1. Introduction

Wildfires release globally significant amounts of aerosols, trace gases, and greenhouse gases that influence air quality, weather, and climate (Bowman et al., 2009; van der Werf et al., 2010). Researchers have devoted considerable efforts to modeling and estimating biomass burning emissions over the last several decades. Pyrogenic emissions are modeled conventionally in a bottom-up manner using information on the burned area, fuel load, combustion completeness (CC), and fuel emission factors (Seiler & Crutzen, 1980). These parameters can be challenging to quantify accurately. For example, burned area estimates can differ by several orders of magnitude (Boschetti et al., 2004; Kasischke et al., 2011; Randerson et al., 2012); fuel loadings may differ by more than 35% among different fuel data sets (Zhang et al., 2008); CC could vary by more than 40% with fuel moisture content in the same fuelbed (Hély et al., 2003); many emission factors also have an uncertainty of about 20–30% (Andreae & Merlet, 2001).

Top-down pyrogenic emission estimation methods have been developed that use satellite retrievals of the instantaneous radiative energy released from actively burning fires detected at the time of satellite overpass. The retrieved instantaneous radiative energy is termed the fire radiative power (FRP) (units: MW). The FRP is proportional to the rate of biomass consumption, and temporal integration of the FRP over the life of the fire provides an estimate of the fire radiative energy (FRE) (units: MJ), which has been shown to be linearly related to the total amount of fuel consumed by fire (Kaufman et al., 1996; Wooster et al., 2003). A scalar constant is used to convert the FRE to the total amount of biomass consumed, termed, for convenience in this paper, the FRE biomass combustion coefficient (FBCC) (units: kg/MJ). The top-down FRE-based emission estimation approach has been used to estimate biomass combustion from FRP retrieved from the polar-orbiting Moderate Resolution Imaging Spectroradiometer (MODIS) and the geostationary Spinning Enhanced

Visible and Infrared Imager for active fires detected at regional to continental scales (Ellicott et al., 2009; Kaiser et al., 2012; Roberts & Wooster, 2008; Vermote et al., 2009; Zhang et al., 2012) and from the Geostationary Operational Environmental Satellites (GOES) across the Conterminous United States (CONUS) (Zhang et al., 2012; Zhang, Kondragunta, & Roy, 2014). The FBCC value is usually assumed to be fixed and has been derived by statistical comparison of FRE retrievals with biomass consumed measurements for prescribed fires lit in the field and under more controlled conditions in plume towers. Studies indicate that the FBCC has a value ranging from 0.368 to 0.453 kg/MJ (Freeborn et al., 2008; Kremens et al., 2012; Wooster et al., 2005). However, the range of fuel types considered in these experiments was limited, primary savanna grass (Wooster et al., 2005); evergreen tree species including ponderosa pine, white pine, and Douglas fir (Freeborn et al., 2008); and mixed oak (Kremens et al., 2012). In addition, the scale of prescribed fires in the field experiments (1.8–64 m^2 plots; Kremens et al., 2012; Wooster et al., 2005) was much reduced compared with landscape wildland fires. At more synoptic scales, using satellite data and models, the FBCC is suggested as varying from 0.30 to 0.52 kg/MJ in Siberia wildfires based on MODIS FRP and satellite-based carbon monoxide (CO) retrievals (Konovalov et al., 2014), as varying from 0.13 to 1.55 kg/MJ based on comparison of MODIS FRE with global biomass combustion estimates from the Global Fire Emissions Database (Kaiser et al., 2012), and as varying from 1.6 to 12.0 kg/MJ (Zhang et al., 2012) based on the comparison of MODIS-based emissions coefficients and aerosol optical thickness data (Ichoku & Kaufman, 2005; Sofiev et al., 2009).

This study quantifies the FBCC at a landscape scale, across the CONUS, by comparing polar-orbiting (MODIS) and geostationary (GOES) satellite-retrieved FRE estimates with biomass combustion estimates for 445 wildland fire events from 2011 to 2012. The biomass consumption estimates were derived using Landsat 30 m burned area maps combined with fuel load information from the Fuel Characteristic Classification System (FCCS) and CC information parameterized with Landsat-derived burn severity estimates. The FBCC was estimated by linear regression of the biomass consumption estimates against the satellite FRE estimates. Sensitivity analyses were undertaken to examine the FBCC variation using the biomass consumptions calculated from a consistent CC in all burn severity classes and from a land-cover-driven approach endorsed for national emission estimation (Intergovernmental Panel on Climate Change (IPCC), 2006). The paper concludes with a discussion of the findings and an appropriate FBCC value for large area satellite FRE-based quantification of biomass combustion.

2. Methods and Data

2.1. Bottom-Up Estimation of Biomass Consumption

Biomass consumption is conventionally estimated as the product of the burned area, fuel load, and CC (Seiler & Crutzen, 1980). In this study we also incorporate the burn severity and assume that burn severity is related positively to biomass consumption for the same fuel type. This is reasonable as fires that burn more biomass are generally expected to have more severe postfire effects (Heward et al., 2013; Keeley, 2009; Smith & Wooster, 2005; Veraverbeke & Hook, 2013). The burn severity is a qualitative metric that reflects the degree of organic matter consumption from fire and relates to changes in living and dead biomass, soil exposure, fire byproducts (char and ash), and fire effects (e.g., scorch height) (Eidenshink et al., 2007; Keeley, 2009). Several of these parameters are not amenable to optical wavelength remote sensing and/or may not be related in a linear way to reflectance (Disney et al., 2011; Roy et al., 2006); however, satellite estimates of burn severity have been widely adopted (Meigs et al., 2009; Moody et al., 2008; Rocha & Shaver, 2011), although with variable results (French et al., 2008; Lentile et al., 2006). In this study, the biomass consumption in a burned area was estimated as

$$\mathrm{BC}_{AMC} = \sum_{i=1}^{n}\sum_{k=1}^{3} A(i,k)M(i,k)C(i,k) \quad (1)$$

where BC_{AMC} is biomass consumption (kg), for fuelbed category i and burn severity class k; $A(i, k)$ is the area burned (km^2); $M(i, k)$ is the fuel loading (kg/km^2); $C(i, k)$ is the CC (unitless: 0–1); and n is the number of fuelbed categories, and there are three burn severity classes. The derivation of these four variables is described below.

2.1.1. Burned Area and Severity

Landsat data have been used for decades to map the spatial extent of burning and to characterize postfire effects (Boschetti et al., 2015; Hawbaker et al., 2017; Lentile et al., 2006). In this study, data from the U.S.

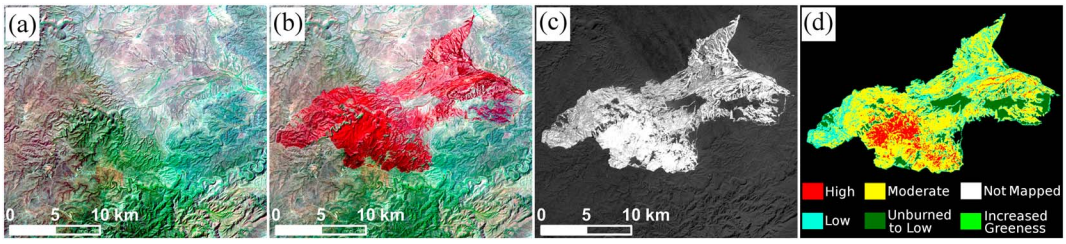

Figure 1. MTBS burn severity example derived from two Landsat images of the 2011 Last Chance fire, New Mexico, USA. (a) Prefire (23 April 2011) Landsat 5 Thematic Mapper false color image (bands 7: 2.08–2.35 μm, 4: 0.76–0.90 μm, and 2: 0.52–0.60 μm). (b) Postfire (9 May 2011) false color image. (c) Differenced normalized burn ratio between the prefire and postfire normalized burn ratio. (d) MTBS burn severity map.

Monitoring Trends in Burn Severity (MTBS) project are used. The MTBS project uses Landsat 30 m Thematic Mapper and Enhanced Thematic Mapper Plus data to map the burn perimeter and the burn severity for all burned areas >404 and >202 ha in the western and eastern CONUS, respectively (Eidenshink et al., 2007). The MTBS project produces 30 m burn severity maps (e.g., Figure 1) by visual interpretation of the temporal difference in the normalized burn ratio (NBR), defined as the difference between the Landsat near-infrared band (0.76–0.90 μm) and the shortwave-infrared band (2.08–2.35 μm) divided by their sum, and a relativized temporal NBR difference (Cocke et al., 2005; Epting et al., 2005; Key & Benson, 2005). The MTBS burn severity map is classified into low, moderate, or high severity classes, with an additional unburned or undetected low severity class and an increased greenness (increased postfire vegetation response) class (Eidenshink et al., 2007). A mask of unprocessed areas (due to cloud obscuration or land not sensed by Landsat) is also provided.

In this study, all the MTBS burned areas defined across the CONUS for 2011 and 2012 were obtained from the MTBS project (http://www.mtbs.gov/). A total of 2616 MTBS burned areas were available, although the final number of burned areas used in the study was reduced to 445 due to the filtering applied (section 2.3).

In equation (1) the area burned (km^2) for an MTBS burned area was derived as the product of the 30 m pixel area (9×10^{-4} km^2) and the sum of the number of 30 m pixels in each of the three (low, moderate, and high) burn severity classes and the fuelbed categories (see section 2.1.2). The unburned or undetected low severity and the increased greenness classes were excluded in the area burned calculation. The areas masked as unprocessed by MTBS were allocated to the three different severity classes (low, moderate, and high severity) weighted by the ratio of the area of a severity class to the total MTBS severity mapped area (as it is reasonable to assume that the burning conditions in the masked areas were similar to those in the processed areas).

2.1.2. Fuel Load

Development of fuel load maps is an area of active research, particularly at national to global scale (Pettinari & Chuvieco, 2016). The FCCS is commonly used because it includes a wide set of fuel physical characteristics that are not specific to a particular application or fire model. The United States FCCS 3.0 provides quantitative fuelbed information compiled from multiple sources including in situ fuel data sets, photographs, literature, and expert knowledge (Ottmar et al., 2007; Prichard et al., 2013). It defines a fuelbed as a set of fuel characteristics on the landscape that represent a distinct combustion environment. There are 250 fuelbeds, and each is divided into six strata with up to 18 categories: tree overstory, tree midstory, tree understory, total trees canopy, shrub, duff, nonwoody (dead and live) vegetation, sound woody debris (0–0.25 [0–0.6], 0.25–1 [0.6–2.54], 1–3 [2.54–7.62], 3–9 [7.62–23], 9–20 [23–51], and >20 [51] cm), and rotten woody debris (3–9 [7.62–23], 9–20 [23–51], and >20 [51] cm) (Ottmar et al., 2007). Each stratum has one or more than one fuelbed category, and each category has common combustion characteristics. The FCCS data set has been used to model surface fire behavior, to predict fire potentials and effects (Cruz & Alexander, 2010; Lutes et al., 2009), and to estimate fuel consumption (FC) and fire emissions (Anjozian, 2009; Ottmar et al., 2006). In this study, the 30 m FCCS fuelbed map for year 2008 and the associated lookup table of fuel loadings per fuelbed category were obtained from the FCCS site (http://www.fs.fed.us/pnw/fera/fccs/maps.shtml).

In equation (1) the mean fuel loading of each fuelbed category and burn severity class was derived as

Table 1
Combustion Completeness Lookup Table Defined as a Function of the Fuelbed Category and Burn Severity Class

Fuelbed		Combustion completeness			
Stratum	Category	Low severity	Moderate severity	High severity	References
Tree canopy	Overstory	0.20	0.45	0.75	Campbell et al. (2007); Ghimire et al. (2012)
	Midstory	0.20	0.50	0.80	
	Understory	0.25	0.60	0.85	
Shrubs		0.30	0.70	0.90	Campbell et al. (2007); De Santis and Chuvieco (2009); Key and Benson (2006)
Non-woody vegetation	Live	0.30	0.88	0.98	Campbell et al. (2007); De Santis and Chuvieco (2009); Key and Benson (2006)
	Dead	0.70	0.90	1.00	
Duff	<4 inches (10.16 cm)	0.50	0.80	0.95	Campbell et al. (2007); Ghimire et al. (2012)
Sound woody debris	<0.25 inches (0.6 cm)	0.70	0.90	1.00	Campbell et al. (2007); Ghimire et al. (2012)
	0.25–1 inch (0.6–2.54 cm)	0.65	0.88	1.00	
	1–3 inches (2.54–7.62 cm)	0.60	0.80	0.85	
	3–9 inches (7.62–23 cm)	0.56	0.63	0.80	
	9–20 inches (23–51 cm)	0.56	0.63	0.80	
	>20 inches (51 cm)	0.20	0.60	0.75	
Rotten woody debris	3–9 inches (7.62–23 cm)	0.56	0.63	0.80	Campbell et al. (2007); Ghimire et al. (2012)
	9–20 inches (23–51 cm)	0.20	0.40	0.65	
	>20 inches (51 cm)	0.20	0.40	0.65	

$$M(i,k) = \frac{\sum_{j=1}^{s} A(i,k,j)FL(i,k,j)}{A(i,k)} \quad (2)$$

where $M(i, k)$ and $A(i, k)$ are the mean fuel loading (kg/km^2) and the area burned (km^2), respectively, in burn severity class k and fuelbed category i over the burned area; j is one of the fuelbeds (a total number of s, $s \leq 250$) that include the fuelbed category i; and $A(i, k, j)$ and $FL(i, k, j)$ are the area burned (km^2) and the fuel loading (kg/km^2), respectively.

Change in the fuelbeds and associated fuel loadings between the production year of the FCCS map and the year of the burn due to land use change, disturbance (previous fires, insects, and drought, etc.), and vegetation seasonal phenology may introduce uncertainty into the biomass consumption estimates. Consequently, the sensitivity of FBCC to the biomass consumption was tested (section 2.5).

2.1.3. Combustion Completeness

The CC, that is, the proportion (0 to 1) of biomass consumed as a result of fire, is dependent on the fuel characteristics, including fuel moisture content, fuel arrangement, and fuel surface area to volume ratio, and environmental conditions (temperature, relative humidity, wind velocity, and slope) that affect the fire behavior and the fire duration (Hély et al., 2003; Ito & Penner, 2004; Ward et al., 1996). It is very challenging to obtain reliable spatially explicit CC maps at landscape scale (Veraverbeke & Hook, 2013). In the absence of any definitive spatially explicit CC data, published lookup tables that define CC as a function of the fuelbed category and burn severity class were used in this study (Table 1). The published CC values were obtained by qualitative field-based assessments of burn severity in the United States (Campbell et al., 2007; De Santis & Chuvieco, 2009; Ghimire et al., 2012; Key & Benson, 2006), typically inferred by human assessments and codified via the composite burn index (CBI) (Key & Benson, 2006) or the modified CBI (GeoCBI) (De Santis & Chuvieco, 2009). The CBI and GeoCBI indices provide a score from 0 to 3, based on fire manager and ecologist qualitative observations of a variety of postfire effects including FC, change in soil color, foliage alteration, change in plant cover, canopy mortality, and scorch height (De Santis & Chuvieco, 2009; Key & Benson, 2006). The CBI and GeoCBI have been shown to be proportional to satellite-derived NBR and differenced normalized burn ratio values but with variable levels of statistical similarity (De Santis & Chuvieco, 2009; French et al., 2008; Keeley, 2009; Lentile et al., 2006; Veraverbeke & Hook, 2013) and as noted earlier some of the postfire effects may not be apparent in optical wavelength data and/or related in a linear way to reflectance (Disney et al., 2011; Roy et al., 2006).

The CC values listed in Table 1 were applied for fuelbed category i and burn severity class k as equation (1) and assuming that the CC was the same for each fuelbed category and burn severity class across each

MTBS burn and for all the burns considered across the CONUS. The sensitivity of FBCC to CC was also tested (section 2.5).

2.2. Top-Down Estimation of Biomass Consumption

Biomass consumption was derived in a top-down way from satellite (MODIS or GOES) estimates of FRE derived over each MTBS burned area (Wooster, 2002; Wooster et al., 2005) as

$$BC_{FRE} = \beta \quad FRE \tag{3}$$

where BC_{FRE} is biomass consumption (kg), β is the FBCC (kg/MJ), and the FRE is the MODIS or GOES FRE (MJ) defined as below.

2.2.1. MODIS FRE Estimation

The global Collection 5 MODIS 1 km Level 2 active fire product detects the 1 km location and time of fires that are burning at the time of overpass of the NASA Terra (MOD14) and Aqua (MYD14) satellites under cloud-free conditions (Giglio, 2013; Giglio et al., 2003). In this study, MOD14 and MYD14 active fire products for 2011–2012 were obtained from the NASA Reverb data portal (http://reverb.echo.nasa.gov/). The products contain for each 1 km pixel whether an active fire was detected, the detection confidence, the FRP (MW), the MODIS band 21 (3.660–3.840 μm) and band 31 (10.780–11.280 μm) blackbody temperatures (K), and average blackbody temperature in these two bands of the surrounding pixels. The MODIS FRP is calculated from band 21 brightness temperature based on a modeled relationship developed in the Smoke, Clouds, and Radiation (SCAR) field experiments (Kaufman et al., 1998). If no MODIS active fire was detected then the surface status (land, water, cloud, or unknown) is defined. Only the nominal- and high-confidence fire detections were considered in this study to remove uncertain active fire detections that are classified as low-confidence detections in the Collection 5 MODIS active fire product (Giglio, 2013). Low-confidence detections are likely to be associated with the false alarms, for example, associated with solar heated charred ground surrounded by cool unburned areas. The Level 2 products are defined in the MODIS orbit geometry, corresponding to approximately 5 min of sensing in the track direction, covering an area of approximately 2,340 by 2,030 km in the across- and along-track directions, respectively. The MODIS scans ten 1 km pixel scan lines per mirror rotation over ±55° and the dimensions of the sensed pixel increase from ~1 km at nadir to ~2.01 km along track and ~4.83 km along scan at the scan edge (Wolfe et al., 1998, 2002). This geometry and the MODIS point spread function can result in the same single fire event being detected two or three times in consecutive scans (Freeborn et al., 2014; Peterson et al., 2013). Accordingly, detections in consecutive scans were considered as duplicated and were removed if they meet the following conditions: (1) detected at the same satellite view angles, (2) difference in observing time is less than 1 min, and (3) distance between two fire pixels is shorter than the along-track dimension of the fire pixels. After this filtering, there are, at CONUS latitudes, a maximum of four MODIS active fire detection opportunities (acquired approximately at 1:30, 10:30, 13:30, or 22:30 local time).

The MODIS FRP is underestimated at greater scan angle because the observed pixel size increases with scan angle (Freeborn et al., 2011; Kumar et al., 2011). To mitigate this effect, the FRP values were adjusted as

$$FRP_{adj} = FRP_{obs} \times \varepsilon \tag{4}$$

where FRP_{adj} is the adjusted FRP (MW), FRP_{obs} is the MODIS retrieved FRP (MW) stored in MOD14 or MYD14, and ε is a published adjustment factor (unitless) defined as a function of the scan angle (Freeborn et al., 2011).

The FRE was estimated from the adjusted MODIS FRP according to the established trapezoid method (Boschetti & Roy, 2009). The method can be applied to estimate FRE at a pixel level or for a cluster of pixels within a burned area. In this study, a cluster is considered as all the MODIS active fire pixels (and associated FRP values) within an MTBS burn perimeter over the life time of the fire. First, the cluster-level FRP was derived as

$$FRP(t_s) = \sum_{m=1}^{u} FRP_{adj}(m, t_s) \tag{5}$$

where $FRP(t_s)$ is the cluster-level FRP (MW) at time t_s when either MODIS sensor detected a fire, $FRP_{adj}(m, t_s)$ is the adjusted FRP of the mth fire pixel (equation (4)), and u is the total number of active fire pixels detected by MODIS at time t_s within an MTBS burned perimeter. Then, the MODIS FRE was derived as

$$\mathrm{FRE} = \sum_{g=1}^{p} \sum_{s=1}^{q-1} \frac{[\mathrm{FRP}(g, t_{s+1}) + \mathrm{FRP}(g, t_s)](t_{s+1} - t_s)}{2} \quad (6)$$

where FRE is the MODIS FRE (MJ) released over the life of the fire in the MTBS burned area, q is total number ($q = 4$) of MODIS observing opportunities on the gth day, p is the total number of days that a fire event lasted, and FRP(g, t_s) is the cluster-level FRP (equation (5)) at time t_s (seconds from 12:00 a.m. local time) on the gth day. Note that FRP(g, t_s) was set to zero if there was no active fire detection on the gth day at time t_s.

2.2.2. GOES FRE Estimation

The GOES-West and GOES-East satellites each sense the CONUS every half an hour (or every 5–15 min in subregions) with a 4–7 km spatial resolution depending on the sensed CONUS location. The WildFire Automated Biomass Burning Algorithm (WF_ABBA Version 65) active fire product defines the location and timing of fires sensed by the GOES geostationary satellites (Prins et al., 1998; Schmidt & Prins, 2003). It provides the active fire detection date and time, geographic coordinate, pixel area, the FRP (MW), ecosystem type, and a quality flag. The FRP is calculated from the middle infrared band (3.9 μm) using the method developed in (Wooster et al., 2003). The WF_ABBA-based GOES fire products for 2011–2012 were obtained from the National Oceanic and Atmospheric Administration (NOAA) (http://satepsanone.nesdis.noaa.gov/pub/FIRE/forPo/).

Successful GOES FRP retrievals are often temporally sparse due to cloud obscuration and sensor saturation (Prins et al., 1998). Therefore, the GOES FRP data were adjusted using the method described in (Zhang et al., 2012). The mean 15 min GOES FRP was defined independently for five ecosystems: forest, savanna, shrubland, grassland, and cropland, providing one mean CONUS FRP value every 15 min per ecosystem. The five ecosystems cover all of the CONUS and were defined by the International Geosphere-Biosphere Programme ecosystem classification (Loveland et al., 2000). The resulting FRP ecosystem-specific 15 min diurnal climatologies were used to adjust the 2010–2012 good quality FRP values over each MTBS burned area using a least squares approach (Zhang et al., 2012). For brevity, we refer to the adjusted FRP time series data as the pixel-level GOES FRP data.

All the pixel-level GOES FRP data within an MTBS burn perimeter were considered as a cluster. The cluster-level GOES FRP over a burned area was calculated as

$$\mathrm{FRP}(t) = \sum_{e=1}^{v} \mathrm{FRP}(t, e) \quad (7)$$

where FRP(t) is the cluster-level GOES FRP (MW), FRP(t, e) is the eth pixel-level FRP (MW) at GOES observation time t, and v is the total number of GOES active fire detections at that time within the MTBS burned perimeter.

It is well established that MODIS is able to detect smaller and cooler fires than GOES due primarily to the higher spatial resolution and also dedicated active detection capabilities of MODIS (Freeborn et al., 2009; Roberts et al., 2005). Consequently, the following adjustment was applied:

$$\mathrm{FRP}_{\mathrm{adj}}(t) = \mathrm{FRP}(t) + \mathrm{FRP}_{\mathrm{offset}}(t) \quad (8)$$

where $\mathrm{FRP}_{\mathrm{adj}}(t)$ is the adjusted GOES cluster-level FRP (MW); FRP(t) is the cluster-level GOES FRP calculated from equation (7), at GOES observation time t; and $\mathrm{FPR}_{\mathrm{offset}}(t)$ is an FRP offset value at time t derived from the difference between the cluster-level MODIS and GOES FRP values (equations (5) and (7)) for that day. $\mathrm{FPR}_{\mathrm{offset}}(t)$ was determined based on the following steps. First the difference between the cluster-level MODIS FRP and the temporally closest cluster-level GOES FRP value was calculated for each MODIS observation during a 24 hr period, termed for brevity $\mathrm{FPR}_{\mathrm{offset}}(t_{\mathrm{MODIS}})$, where t_{MODIS} is the MODIS observing local time (t_{MODIS} is approximately one of 1:30, 10:30, 13:30, or 22:30). If there were no MODIS FRP data over the burn in a 24 hr period then $\mathrm{FPR}_{\mathrm{offset}}(t)$ was set to zero for the period. If there were one or two MODIS FRP values in the 24 hr period then $\mathrm{FPR}_{\mathrm{offset}}(t)$ was set as the average of the $\mathrm{FPR}_{\mathrm{offset}}(t_{\mathrm{MODIS}})$ values. If there were more than two MODIS FRP values then the $\mathrm{FPR}_{\mathrm{offset}}(t)$ was set to the first $\mathrm{FPR}_{\mathrm{offset}}(t_{\mathrm{MODIS}})$ value for all times before the first MODIS observation in the day, or was linearly interpolated in time from the two closest $\mathrm{FPR}_{\mathrm{offset}}(t_{\mathrm{MODIS}})$ values for times between the MODIS observations, or was set to the last $\mathrm{FPR}_{\mathrm{offset}}(t_{\mathrm{MODIS}})$ value in the day for all times after the last MODIS observation. The results of this process are illustrated in Figure 2 for four cases showing different numbers of MODIS active fire detections in a 24 hr period.

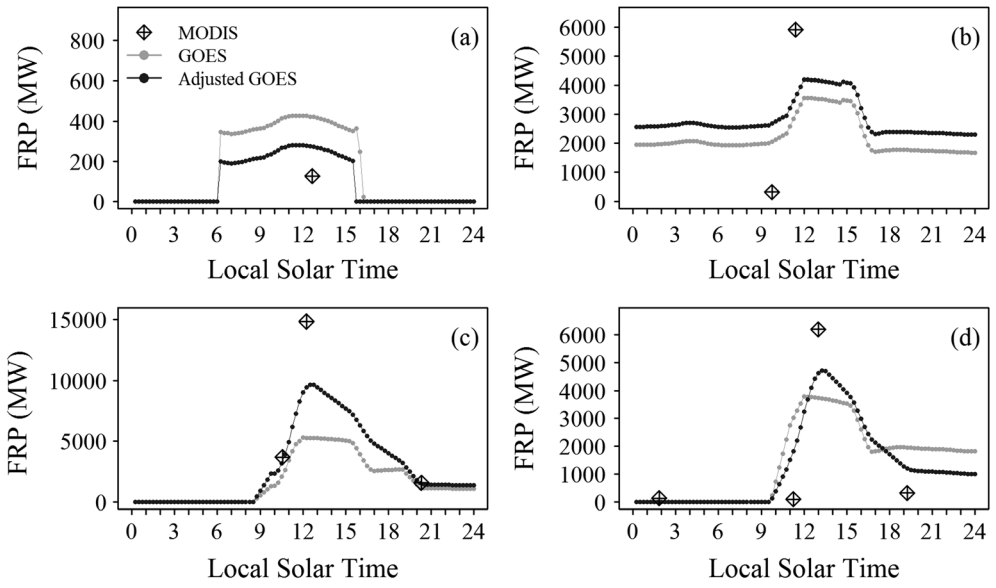

Figure 2. Illustration of the adjustment of cluster-level GOES FRP) over a 24 hr period for four examples where there are (a) one, (b) two, (c) three, and (d) four contemporaneous cluster-level MODIS FRP values. The gray and black filled cycles show the cluster-level GOES FRP before and after the adjustment, respectively, and the diamonds show the cluster-level MODIS FRP. The examples show satellite data for 23 August, 27 August, 30 July, and 1 September 2012, respectively, acquired over the Halstead fire, Idaho, USA.

The FRE was estimated from the adjusted GOES FRP for each MTBS burned area as

$$\mathrm{FRE} = \sum_{d=1}^{n} \sum_{t=1}^{96} \left[\mathrm{FRP}_{\mathrm{adj}}(t) \times 900\right] \tag{9}$$

where FRE is the GOES FRE (MJ) released over the life of the fire in the MTBS burned area, n is the total number of days that the fire event lasted, and $\mathrm{FRP}_{\mathrm{adj}}(t)$ is defined as equation (8) for every 15 min (corresponding to 900 s), and there are 96 15 min periods each day (24 hr). This implicitly assumes that a fire event burned consistently in the same way in each 15 min period (Zhang et al., 2012).

2.3. Processing of Data to Ensure Contemporaneous Observations

The MTBS burned area perimeters were intersected spatially with the locations of the MODIS and GOES active fire detections so that the satellite FRE could be compared with the Landsat-derived biomass consumption (equation (1)) for each MTBS burned area. Specifically, the satellite active fire detections were projected into the Universal Transverse Mercator (UTM) projection defining the MTBS fire perimeter data. Each burned area perimeter was buffered outward by 5 km to accommodate for the coarser spatial resolution of the 4 km GOES active fire detections relative to the 1 km MODIS detections. All the active fire detections located within each buffered perimeter were considered within 80 days after the date of fire ignition defined in the MTBS burn metadata. An 80 day temporal threshold was used as several extensive CONUS fires lasted up to two months. This process is illustrated in Figure 3, which shows an example where active fire detections of GOES and MODIS were spatially and temporally intersected with an MTBS burned area.

All MTBS burned areas with insufficient active fire detections were removed from the analysis. To do this, the geographic spatial coverage of the active fire detections was derived as the spatial union of all the fire detection pixel areas within the 5 km buffered MTBS burned area over 80 days. The GOES fire pixel area was obtained from the WF_ABBA Version 65 GOES active fire product, and the MODIS fire pixel area was calculated using the MODIS along-scan and along-track pixel dimensions (Giglio, 2013). For these two sensors, their pixel areas increase as scan angle increases from nadir to scan edge and the pixel shapes were approximated with rectangles in this study. For instance, for a MODIS fire pixel, its along-scan and along-track pixel dimensions were taken as the product of the length and width of the rectangle. The burned area was rejected from consideration if the geographic spatial coverage of the active fire detections was less than 85% of the area mapped by MTBS as low, moderate, and high burn severity. The 85% threshold was set quite

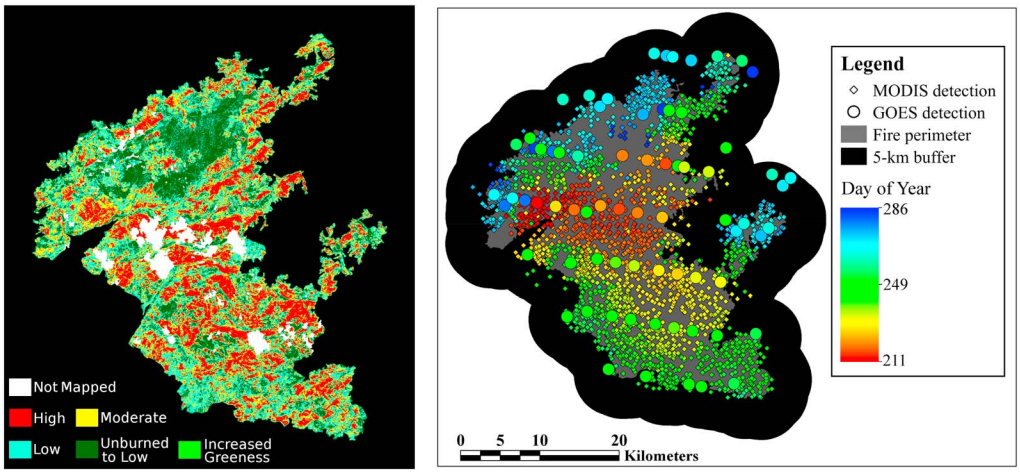

Figure 3. Spatial and temporal match of MTBS Landsat burned area and severity classes (left) with MODIS and GOES active fire detections (right) for the Halstead fire in Idaho, 2012.

conservatively to prevent satellite FRE from being grossly underestimated due to insufficient FRP sampling, although burned areas containing persistently burning active fires (i.e., forested systems) are less likely to be rejected. A total of 445 burned areas were selected in this way.

2.4. Estimation of the FRE Biomass Combustion Coefficient (FBCC)

The bottom-up (BC_{AMC}; equation (1)) and top-down (BC_{FRE}; equation (3)) biomass consumption estimates should equal the actual biomass consumption over the same fire event if the models, assumptions, and parameters, implicit in their derivations, are correct. In this study, we assume that this is the case, that is, that BC_{AMC} equals BC_{FRE}, and so rearranging equations (1) and (3) provides

$$BC_{AMC} = FBCC \times FRE \tag{10}$$

where BC_{AMC} is the biomass consumption (kg) derived as equation (1), FRE is the satellite derived FRE (MJ) defined by equation (6) (MODIS FRE) or equation (9) (GOES FRE), and FBCC is the FBCC (kg/MJ).

The FBCC was derived by linear ordinary least squares regression of the BC_{AMC} (dependent variable) and satellite FRE estimates (independent variable) for the 455 CONUS burned areas and forcing the regression to have a zero intercept value. This was undertaken three times: considering the MODIS FRE, the GOES FRE, and the average of the MODIS and GOES FRE derived for each burn. The regression coefficient of determination (r^2) and p-value were used to test the statistical significance of the FBCC regression coefficients.

2.5. Sensitivity Analysis

There are several possible error sources that are discussed in the discussion. As there are no independent satellite FRE, or ground truth FC data, for the 455 MTBS burned areas, only a limited sensitivity analysis could be undertaken. Two sensitivity analyses of the bottom-up biomass consumption estimation were conducted.

First, the CC parameterization with respect to burn severity (Table 1) was replaced with a single CC of 0.5, that is, simply assuming that half of the fuel load burned regardless of the fuel type or the burn severity. This value was used because it is close to the median value in Table 1. The biomass consumption (BC_{AMC}) was then calculated as equation (1) for the 445 selected MTBS burned areas using CC = 0.5 and the FCCS fuel loadings as before.

Second, the biomass consumption was computed in a different way using a land-cover driven approach endorsed for national emissions estimation (IPCC, 2006) defined as

$$BC_{AMC} = \sum_{l=1}^{h} A(l)FC(l) \tag{11}$$

where BC_{AMC} is biomass consumption (kg) in the MTBS burned area; there are a total of h land cover types in

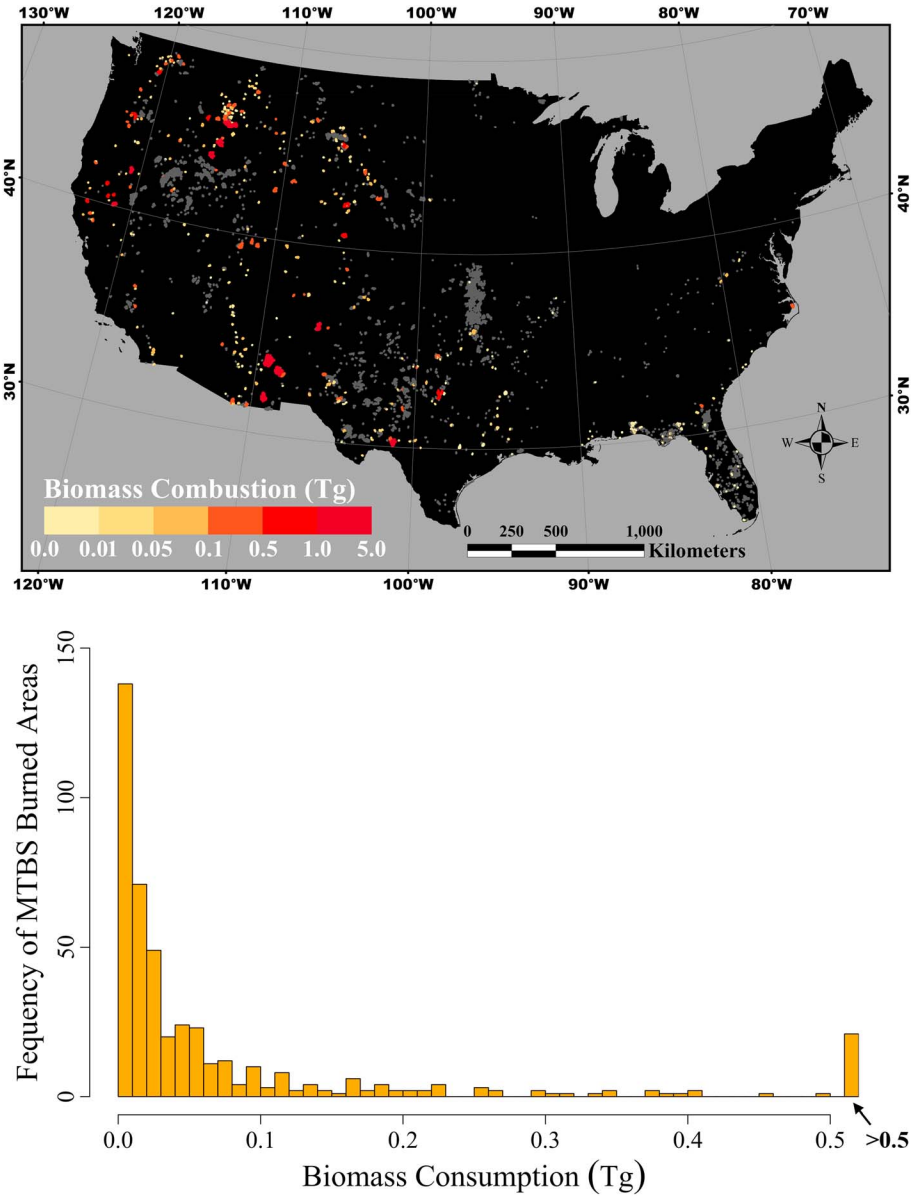

Figure 4. The selected 2011 and 2012 CONUS MTBS burned areas (total 445, orange and red colors) and the biomass consumption estimated by the bottom-up method (equation (1)) based on the burn severity parameterized combustion completeness. (top) The spatial distribution of the biomass consumption in the selected 445 burned areas (colored polygons); the gray polygons show the other 2011 and 2012 available MTBS burned areas that were not considered as they did not have sufficient contemporaneous MODIS and GOES active fire detections (see section 2.3). (bottom) The histogram of the biomass consumption in the selected 445 burned areas.

the burned area and the *l*th land cover type has area burned $A(l)$ (km^2) and fuel consumption $FC(l)$ (kg/km^2). The 30 m National Land Cover Database (NLCD) 2011, which defines 16 land cover classes over the CONUS (Homer et al., 2015) and has a reported overall accuracy of 78.7% (Wickham et al., 2013), was used to define the land cover classes that were intersected (as described above in section 2.3) with each buffered MTBS burned area. The IPCC provides mean FC (units: kg/m^2) for broadly defined land cover types that were derived from published literature estimates (IPCC, 2006). The broadly defined land cover types were cross-walked to NLCD land cover types. Across the 455 burned areas in this study there were only five (nonwater) IPCC unique mean FC values of 0.36 kg/m^2 (woody wetland and herbaceous wetland NLCD classes), 0.376 kg/m^2 (grassland, pasture, and developed open NLCD classes), 0.55 kg/m^2 (crops NLCD classes), 1.43 kg/m^2 (shrub, scrub NLCD classes), and 5.04 kg/m^2 (deciduous, mixed, and evergreen forest

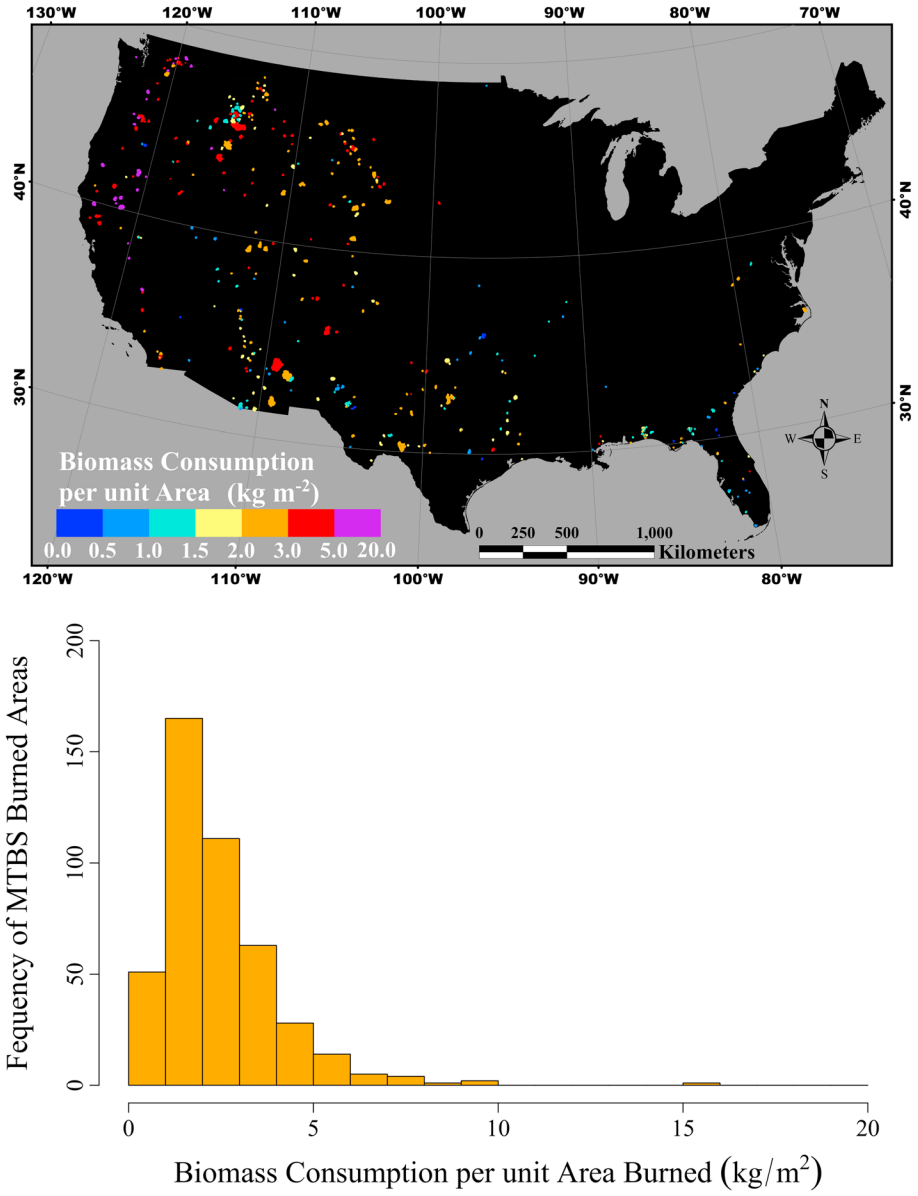

Figure 5. Biomass consumption (Figure 4) per area burned (units: kg/m2) in the selected 2011 and 2012 CONUS MTBS burned areas (total 445). (top and bottom) The spatial distribution and histogram of the biomass consumption per area burned, respectively, across the CONUS.

NLCD classes). The IPCC forest FC estimate used (5.04 kg/m^2) is similar (difference $<$ 8%) to recent field measured U.S. forest mean FC data (van Leeuwen et al., 2014).

3. Results

Figure 4 shows the 445 (229 in 2011 and 216 in 2012) MTBS burned areas, selected because they had contemporaneous MODIS and GOES active fire detections, and their biomass consumption estimated using the bottom-up approach (equation (1)). The 445 MTBS burned areas occurred mainly in the west and southeast CONUS and ranged in area from 1.221 to 1,353.088 km^2. The burned areas in the southeast were generally smaller and varied in size from 1.221 to 45.977 km^2. The largest burn was the Wallow fire in Arizona that burned 1,353.088 km^2 of predominantly mixed conifer forest including ponderosa pine, Douglas-fir, aspen, and Gambel oak (Waltz et al., 2014). The biomass consumption for the 455 burns varied from 2.47×10^{-4} to 4.08 Tg. Larger burned areas tended to have greater biomass consumption. All the burns with more

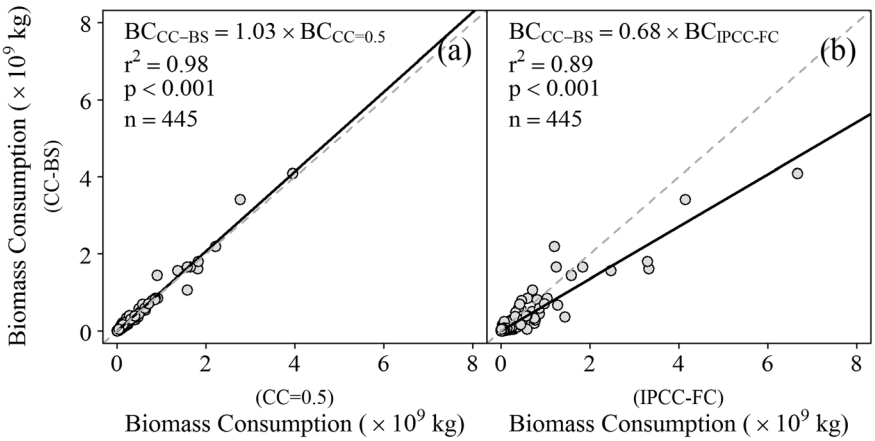

Figure 6. Comparison of the biomass consumption derived using the burn severity parameterized combustion completeness (CC) approach (Figure 4) with (a) the biomass consumption derived using the same method but fixed CC = 0.5 and with (b) the IPCC land-cover-driven approach (equation (11)). Linear regressions of the plotted data (solid lines) and the 1:1 line for comparison (dashed lines) are shown. The regression slope terms are the estimated FBCC values.

than 1.0 Tg consumption occurred in the western CONUS, where the greatest biomass consumption (4.08 Tg) was for the Wallow fire. The MTBS burn severity for the 455 burned areas was quite variable with no clear geographical pattern across the CONUS. The proportions of low, moderate, and high burn severity areas within a burned area on average were 62%, 27%, and 11%, respectively, across the 445 burned areas.

Figure 5 shows the biomass consumption per unit area, found by dividing the biomass consumption (Figure 4) by the area burned. The biomass consumption per unit area was generally smaller in the southeast (<3.0 kg/m^2) and larger in the western states, particularly California, Oregon, and Washington, with values ranging from 1.5 to 20.0 kg/m^2. For the largest Wallow fire, the biomass consumption per unit area was 3.02 kg/m^2 (Figure 5), which differs by only 4% from the biomass consumption estimated using the Consume 3.0 FC model (Veraverbeke & Hook, 2013). The results illustrated in Figure 5 are comparable in magnitude with biomass consumption estimates across the CONUS for different fires and years (where fuel conditions and fire behavior differences mean that exact quantitative comparison is not meaningful; Lydersen et al., 2014; Prichard et al., 2017; Yokelson et al., 2013).

Figure 6 illustrates a comparison of the biomass consumption estimated by the bottom-up method based on the burn severity parameterized CC approach with the same approach but assuming CC = 0.5 (Figure 6a) and with the IPCC FC method (Figure 6b). Linear regression of the results indicates that the different biomass consumption estimates were significantly correlated ($r^2 \geq 0.89$ and $p < 0.001$). The regression slopes indicate that over the 445 sites, the burn severity parameterized biomass consumption estimates were larger by 3% than the CC = 0.5 estimates but 32% smaller than the IPCC-FC-based biomass consumption estimates.

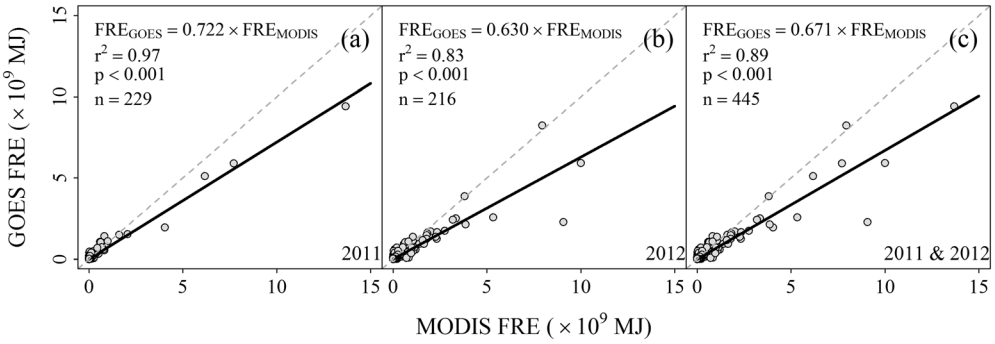

Figure 7. Comparisons between the adjusted cluster GOES FRE (equation (9)) and the cluster MODIS FRE (equation (6)) over the selected burned areas for (a) 2011 (229 burned areas), (b) 2012 (216 burned areas), and (c) for both 2011 and 2012 (445 burned areas). Linear regressions of the plotted data (solid lines) and the 1:1 line for comparison (dashed lines) are shown.

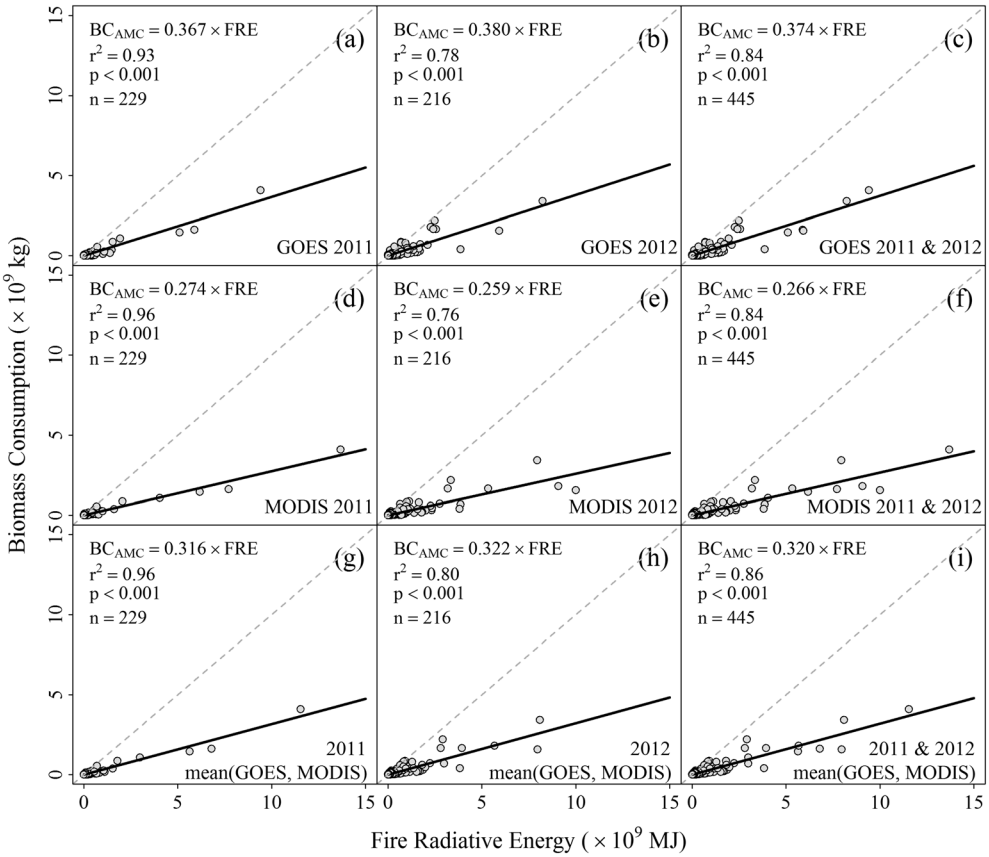

Figure 8. Relationships between the biomass consumption estimated by the burn severity parameterized CC approach (equation (1)) and the adjusted cluster GOES FRE (equation (9)) and the cluster MODIS FRE (equation (6)) and the average of the MODIS and GOES FRE in each burned area, for 2011, 2012, and both years together. Linear regressions of the plotted data (solid lines) and the 1:1 line (i.e., slope of 1.0 kg/MJ) (dashed lines) are shown. The regression slope terms are the estimated FBCC values.

Figure 7 shows, for the burned areas in 2011, 2012, and for both years combined, the relationship between the adjusted cluster GOES FRE and the cluster MODIS FRE. The sensor FRE data were significantly correlated ($r^2 > 0.8$ and $p < 0.001$) and the GOES FRE was about a third less than the MODIS FRE. In Figure 7, the GOES FRE varied from 0.99×10^5 to 9.41×10^9 MJ and the MODIS FRE varied from 5.67×10^5 to 13.68×10^9 MJ. The greatest FRE values were for the 2011 Wallow fire that also had the greatest area burned.

Figure 8 shows the relationships between the biomass consumption estimated by the burn severity parameterized CC approach and the GOES FRE, MODIS FRE, and the average of the GOES and MODIS FRE. The results for the burned areas in 2011, 2012, and for both years combined are shown. In all cases, the data were significantly correlated ($r^2 > 0.75$ and $p < 0.001$). Recall that from equation (10) the slopes of the regressions plotted in Figure 8 provide an estimate of the FBCC. The FBCC estimates from the GOES FRE were larger than those from MODIS FRE by 34% and 46% in 2011 and 2012, respectively. When considering both years, the FBCC estimates were 0.374 kg/MJ for GOES FRE, 0.266 kg/MJ for MODIS FRE, and intermediate (0.320 kg/MJ) for the average MODIS and GOES FRE.

Figure 9 shows the same results as Figure 8 for both years combined (2011 and 2012) but compares the biomass consumption estimated with CC = 0.5 and with the IPCC-FC method against the satellite FRE. All the regressions were significant ($r^2 \geq 0.79$ and $p < 0.001$). When both years were considered, the FBCC values from GOES FRE were larger than those from the MODIS FRE by 37% for both the CC = 0.5 estimation and the IPCC-FC estimation. The FBCC values from the average of GOES and MODIS FRE estimates were 0.301 and 0.458 kg/MJ for the CC = 0.5 estimation and the IPCC-FC estimation, respectively, considering both years. In comparison with the FBCC estimates based on burn severity parameterized CC (Figure 8) when both years were considered, the FBCC values derived assuming CC = 0.5 (Figure 9) were smaller by 7% for GOES FRE and

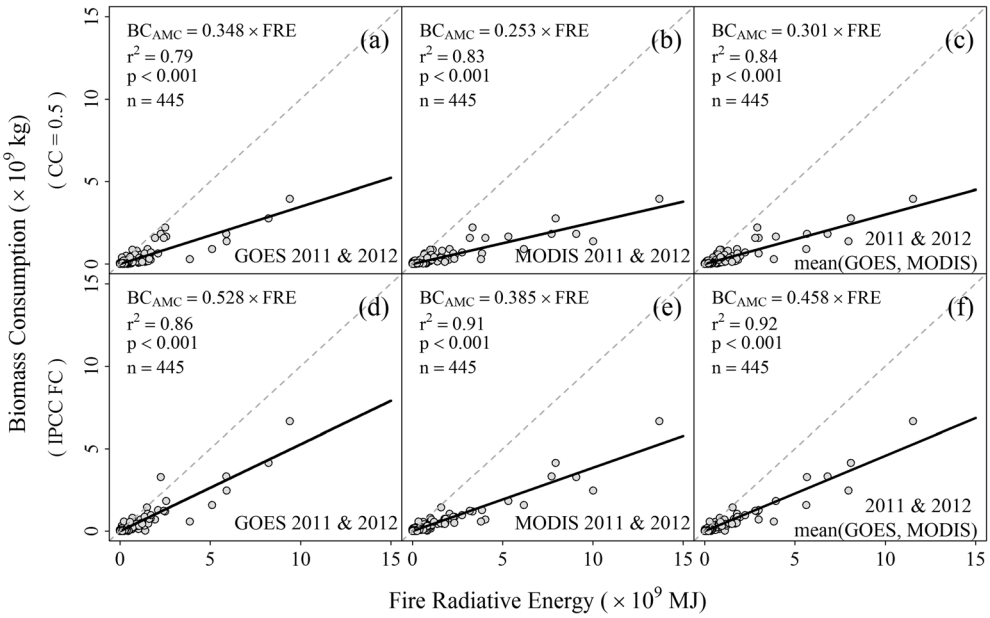

Figure 9. Relationships between the biomass consumption estimated with CC = 0.5 and with the IPCC-FC method with the adjusted cluster GOES FRE (equation (9)) and the cluster MODIS FRE (equation (6)) and the average of GOES and MODIS FRE in each burned area, for 2011, 2012, and both years together. Linear regressions of the plotted data (solid lines) and the 1:1 line (i.e., slope of 1.0 kg/MJ) (dashed lines) are shown. The regression slope terms are the estimated FBCC values.

5% for MODIS FRE, respectively, and the FBCC values derived from the IPCC-FC estimation (Figure 9) were larger by 41% for GOES FRE and 45% for MODIS FRE, respectively.

4. Discussions and Conclusions

This study investigated the relationship between satellite-retrieved FRE and biomass consumption estimates for 445 wildland fire events in 2011 and 2012. This large sample helps to improve our understanding of the FBCC for the estimation of biomass consumption using satellite FRP retrievals. The FBCC bridges the biomass combustion rate to FRP that provides a direct way to quantify biomass consumption (Kaufman et al., 1998; Wooster et al., 2003). The FRE-based top-down approach may be advantageous compared to bottom-up approaches as fuel load and CC information are not required (Roberts et al., 2005; Wooster et al., 2003). However, the FBCC value derived from different approaches is quite variable (0.13 to 12.0 kg/MJ) (Freeborn et al., 2008; Kaiser et al., 2012; Konovalov et al., 2014; Kremens et al., 2012; Wooster et al., 2005; Zhang et al., 2012), which is a concern for the use of satellite FRE-based biomass consumption and biomass burning emission estimation.

The biomass consumption derived for Landsat mapped burned areas using a conventional bottom-up approach (equation (1)) may have considerable uncertainty, even though the best data available, that is, MTBS Landsat burned area and FCCS fuel bed and fuel loading information, were used. The area burned from MTBS is generally considered reliable, but in certain mapped burns the interior unburned areas may not be delineated, although these interior unburned areas typically have low severity (Sparks et al., 2015) that may reduce the impact of MTBS burned area commission errors. The MTBS definition of burn severity is not consistently quantified but rather is based on subjective thresholding of the Landsat NBR that reduces their reliability (Eidenshink et al., 2007). The FCCS fuel loading information are static and so do not reflect seasonal and interannual fuel load changes (Pellizzaro et al., 2007). Moreover, the FCCS information may not reflect the fire history reliably; for example, a fire in the years before 2011 may have reduced the fuel load but may not be reflected in the FCCS (Steel et al., 2015). In addition, although the CC values in Table 1 were compiled from a large number of available forest and nonforest sources (including 15 studies summarized in Ghimire et al., 2012), they may not adequately represent the fire behavior and fuel beds for the 445 fire events and could be augmented using more estimates such as, for example, Lentile et al. (2009). Further, the CC parametrization

by burn severity was simple, although based on empirical evidence of a linear relationship between these measures, and is known to have quite variable results (French et al., 2008; Veraverbeke & Hook, 2013).

In the absence of independent ground-truth biomass consumption data, sensitivity analyses were conducted to examine the sensitivity of the bottom-up biomass consumption estimation. The biomass consumption estimated by the bottom-up method (equation (1)) based on the burn severity parameterized CC was close to that assuming a fixed CC = 0.5 (Figure 6a). We note that CC = 0.5 is only 10% less than the mean of all the CC values parameterized by burn severity class (Table 1) and is about 18% smaller than the average of CC values measured at 15 sites across the CONUS (van Leeuwen et al., 2014). For the fixed CC results potentially large biomass consumption biases may occur if the CC values are very different to the fixed value. This may be the case as across the 445 CONUS burned areas, the proportions of low, moderate, and high burn severity areas were 62%, 27%, and 11%, respectively. We also note that CC and burn severity may not always be directly related. For example, large trees that burn for long periods may result in white ash that are not detected and/or have low Landsat-derived burn severity (Roy et al., 2010; Smith & Hudak, 2005). Similarly, a fire may result in near complete combustion but the Landsat burn severity will not be mapped as high or moderate severity if only a fraction of the pixel is burned (Roy & Landmann, 2005).

Despite these caveats, the utility of the CC parameterization is evident in Figure 6a, which shows the biomass consumption estimates based on the burn severity parameterized CC against the CC = 0.5 based biomass consumption. In this figure two burned areas had biomass consumption estimates that were 59% and 23% greater than when CC = 0.5 was assumed, and these were for burned areas with moderate and high burn severity. Conversely, the one burned area with a biomass consumption estimate particularly below the 1:1 line was a low burn severity fire. Besides the parameterized CC, the need of spatially explicit fuel characteristics at burned area level was also suggested in the comparison of biomass consumption estimates based on the burn severity parameterized CC against those based on the IPCC approach (Figure 6). The biomass consumption estimated using the IPCC land cover-based method was 32% greater than that based on burn severity and had much more scatter (Figure 6b) than the CC = 0.5 based biomass consumption (Figure 6a). This could be due to the significantly simplified IPCC FC approach that is insufficient to characterize individual fire events. The use of only five unique IPCC FC values for the 445 burned areas will provide rather generalized biomass consumption estimates that do not capture variations associated with fire behavior and site conditions.

Researchers have suggested a number of factors that may impact the reliability of satellite FRE retrieval. These include sensitivity to active fire detection capabilities (Giglio et al., 2003), under sampling of active fire events due primarily to the satellite orbit and sensing geometry and also cloud, smoke and overstory vegetation obscuration (Boschetti & Roy, 2009; Freeborn et al., 2014; Kumar et al., 2011; Mathews et al., 2016; Xu et al., 2010), reduction in FRP values due to the absorbing properties of smoke and atmospheric water vapor (Wooster et al., 2005) and fuel moisture (Smith et al., 2013), and issues with the geometric sensing characteristics relative to the spatial configuration and temperatures of actively burning fires (Calle et al., 2009; Freeborn et al., 2014). In this study polar-orbiting MODIS and geostationary GOES FRP data were used to derive the FRE. Compared to GOES, the MODIS is able to detect smaller and cooler fires but no more than four times per day. Conversely, the GOES has the capability to capture the fire diurnal variation due to its 5–15 min sampling but cannot detect small and cool fires (Freeborn et al., 2011; Roberts & Wooster, 2014; Xu et al., 2010; Zhang et al., 2012). In this study, the pixel-level MODIS FRP was adjusted using the method by Freeborn et al. (2011) to mitigate the underestimation of MODIS FRP at off nadir (equation (4)) and aggregated to obtain adjusted cluster-level MODIS FRP (equation (5)). To account for the underestimation of GOES FRP due to missed small and cool fires, the cluster-level GOES FRP estimate at each GOES observing time was adjusted over each of the 455 burned areas by adding an FRP offset (equation (8)) that was calculated from the difference between the cluster-level GOES and adjusted MODIS FRP estimates. The example in Figure 2 illustrates the adjustment of cluster-level GOES FRP in different situations. The cluster-level MODIS FRP and adjusted GOES FRP were applied to estimate adjusted MODIS FRE and adjusted GOES FRE using established temporal integration methods (Boschetti & Roy, 2009; Zhang et al., 2012). The adjusted MODIS and GOES FRE values were significantly correlated across the 445 burned areas, and the GOES FRE was about a third less than the MODIS FRE. Other researchers have noted smaller MODIS FRE than geostationary FRE derived over Africa from the Meteosat Second Generation Spinning Enhanced Visible and Infrared Imager FRE (Freeborn et al., 2011; Vermote et al., 2009) although this could be attributed to different FRE

derivation methodologies, fire regimes, and sensor capabilities. The satellite-derived FRE in this study could not be validated because there are no independent and contemporaneous FRE measurements. The relative error characteristics of the adjusted GOES and MODIS FRE are unknown and so for each burned area their average was taken. Further work to investigate a weighting scheme or some other way to optimally combine the FRE from these the MODIS and GOES sensors is recommended.

Despite the above issues, this study demonstrated that the derived FBCC values were relatively stable. Comparing the satellite FRE with the biomass consumption estimated by the burn severity parameterized CC approach provided FBCC values of 0.374 kg/MJ (GOES), 0.266 kg/MJ (MODIS), and 0.320 kg/MJ (average of GOES and MODIS FRE) when both years (2011 and 2012) were considered for the 445 CONUS fire events, and for either year, the derived FBCC value of one year varied by less than 6% of the other year's value. The other biomass consumption estimation methods considered provided similar magnitude FBCC values, with a two-year average GOES and MODIS FRE estimate of 0.301 kg/MJ when the CC was fixed as 0.5 and 0.458 kg/MJ for the IPCC-based method. All of these values are similar to the FBCC values derived from field and plume tower prescribed fire experiments (0.368–0.453 kg/MJ) (Freeborn et al., 2008; Kremens et al., 2012; Wooster et al., 2005) and also with certain synoptic-scale satellite research (0.300–0.520 kg/MJ) (Konovalov et al., 2014). They are smaller, however, than the FBCC values (0.13–1.55 kg/MJ) estimated using Global Fire Emissions Database and MODIS FRE (Kaiser et al., 2012) and much smaller than the values (1.6–12.0 kg/MJ) derived comparing MODIS-based emission coefficients and aerosol optical thickness data (Sofiev et al., 2009; Zhang et al., 2012). The large discrepancies among FBCC values derived by different approaches may explain some of the discrepancies among the existing FRP-based emission data sets (Zhang et al., 2012; Zhang, Wang, et al., 2014).

In summary, this study confirms the empirical relationship between biomass consumption estimates and FRE for landscape wildland fires. Despite the uncertainties in the data used, it is important to note that for all cases the experiments confirmed the linear relationship between FRE and biomass consumption observed in previous studies (Freeborn et al., 2008; Kremens et al., 2012; Wooster et al., 2005). For combined use of GOES and MODIS FRE, an FBCC value of 0.320 kg/MJ is suggested. Landscape scale and detailed fire event specific experiments are needed. However, this is challenging due to the difficulty in measuring prefire and postfire fuel loads and spatially explicit CC over large burned areas. These challenges might be mitigated by advances in technologies of remote sensing and field measurements, for example, application of LiDAR in estimation of fuel loads from airborne- and ground-based platforms (Cooper et al., 2017; Hudak et al., 2016; Price & Gordon, 2016) over prescribed fires, and also over wildfires if the prefire fuel conditions can be assessed.

Acknowledgments
This research was funded by NOAA contract NA14NES4320003 and BG-133E-15-SE-1613. The manuscript contents are solely the opinions of the author(s) and do not constitute a statement of policy, decision, or position on behalf of NOAA or the U.S. Government. The authors thank reviewers and Editors for their constructive comments. The authors comply with AGU's data policy.

References

Andreae, M. O., & Merlet, P. (2001). Emission of trace gases and aerosols from biomass burning. *Global Biogeochemical Cycles*, *15*(4), 955–966. https://doi.org/10.1029/2000GB001382

Anjozian, L.-N. (2009). Consume 3.0—A software tool for computing fuel consumption. In *Fire Science Brief* (Vol. 55, pp. 1–6). Retrieved from https://www.firescience.gov/projects/briefs/98-1-9-06_FSBrief55.pdf, last accessed on 1/30/2018.

Boschetti, L., & Roy, D. P. (2009). Strategies for the fusion of satellite fire radiative power with burned area data for fire radiative energy derivation. *Journal of Geophysical Research*, *114*, D20302. https://doi.org/10.1029/2008JD011645

Boschetti, L., Eva, H. D., Brivio, P. A., & Grégoire, J. M. (2004). Lessons to be learned from the comparison of three satellite-derived biomass burning products. *Geophysical Research Letters*, *31*, L21501. https://doi.org/10.1029/2004GL021229

Boschetti, L., Roy, D. P., Justice, C. O., & Humber, M. L. (2015). MODIS–Landsat fusion for large area 30 m burned area mapping. *Remote Sensing of Environment*, *161*(0), 27–42. https://doi.org/10.1016/j.rse.2015.01.022

Bowman, D. M. J. S., Balch, J. K., Artaxo, P., Bond, W. J., Carlson, J. M., Cochrane, M. A., et al. (2009). Fire in the Earth system. *Science*, *324*(5926), 481–484. https://doi.org/10.1126/science.1163886

Calle, A., Casanova, J. L., & González-Alonso, F. (2009). Impact of point spread function of MSG-SEVIRI on active fire detection. *International Journal of Remote Sensing*, *30*(17), 4567–4579. https://doi.org/10.1080/01431160802609726

Campbell, J., Donato, D., Azuma, D., & Law, B. (2007). Pyrogenic carbon emission from a large wildfire in Oregon, United States. *Journal of Geophysical Research: Biogeosciences*, *112*, G04014. https://doi.org/10.1029/2007JG000451

Cocke, A. E., Fulé, P. Z., & Crouse, J. E. (2005). Comparison of burn severity assessments using differenced normalized burn ratio and ground data. *International Journal of Wildland Fire*, *14*(2), 189–198. https://doi.org/10.1071/WF04010

Cooper, S., Roy, D., Schaaf, C., & Paynter, I. (2017). Examination of the potential of terrestrial laser scanning and structure-from-motion photogrammetry for rapid nondestructive field measurement of grass biomass. *Remote Sensing*, *9*(12), 531. https://doi.org/10.3390/rs9060531

Cruz, M. G., & Alexander, M. E. (2010). Assessing crown fire potential in coniferous forests of western North America: A critique of current approaches and recent simulation studies. *International Journal of Wildland Fire*, *19*(4), 377–398. https://doi.org/10.1071/WF08132

De Santis, A., & Chuvieco, E. (2009). GeoCBI: A modified version of the composite burn index for the initial assessment of the short-term burn severity from remotely sensed data. *Remote Sensing of Environment*, *113*(3), 554–562. https://doi.org/10.1016/j.rse.2008.10.011

Disney, M. I., Lewis, P., Gomez-Dans, J., Roy, D., Wooster, M. J., & Lajas, D. (2011). 3D radiative transfer modelling of fire impacts on a two-layer savanna system. *Remote Sensing of Environment*, *115*(8), 1866–1881. https://doi.org/10.1016/j.rse.2011.03.010

Eidenshink, J., Schwind, B., Brewer, K., Zhu, Z., Quayle, B., & Howard, S. (2007). A project for monitoring trends in burn severity. *Fire Ecology*, *3*(1), 3–21. https://doi.org/10.4996/fireecology.0301003

Ellicott, E., Vermote, E., Giglio, L., & Roberts, G. (2009). Estimating biomass consumed from fire using MODIS FRE. *Geophysical Research Letters*, *36*, L13401. https://doi.org/10.1029/2009GL038581

Epting, J., Verbyla, D., & Sorbel, B. (2005). Evaluation of remotely sensed indices for assessing burn severity in interior Alaska using Landsat TM and ETM+. *Remote Sensing of Environment*, *96*(3-4), 328–339. https://doi.org/10.1016/j.rse.2005.03.002

Freeborn, P. H., Wooster, M. J., Hao, W. M., Ryan, C. A., Nordgren, B. L., Baker, S. P., & Ichoku, C. (2008). Relationships between energy release, fuel mass loss, and trace gas and aerosol emissions during laboratory biomass fires. *Journal of Geophysical Research*, *113*, DO1301. https://doi.org/10.1029/2007JD008679

Freeborn, P. H., Wooster, M. J., & Roberts, G. (2011). Addressing the spatiotemporal sampling design of MODIS to provide estimates of the fire radiative energy emitted from Africa. *Remote Sensing of Environment*, *115*(2), 475–489. https://doi.org/10.1016/j.rse.2010.09.017

Freeborn, P. H., Wooster, M. J., Roberts, G., Malamud, B. D., & Xu, W. (2009). Development of a virtual active fire product for Africa through a synthesis of geostationary and polar orbiting satellite data. *Remote Sensing of Environment*, *113*(8), 1700–1711. https://doi.org/10.1016/j.rse.2009.03.013

Freeborn, P. H., Wooster, M. J., Roy, D. P., & Cochrane, M. A. (2014). Quantification of MODIS fire radiative power (FRP) measurement uncertainty for use in satellite-based active fire characterization and biomass burning estimation. *Geophysical Research Letters*, *41*, 1988–1994. https://doi.org/10.1002/2013GL059086

French, N. H. F., Kasischke, E. S., Hall, R. J., Murphy, K. A., Verbyla, D. L., Hoy, E. E., & Allen, J. L. (2008). Using Landsat data to assess fire and burn severity in the north American boreal forest region: An overview and summary of results. *International Journal of Wildland Fire*, *17*(4), 443–462. https://doi.org/10.1071/WF08007

Ghimire, B., Williams, C. A., Collatz, G. J., & Vanderhoof, M. (2012). Fire-induced carbon emissions and regrowth uptake in western U.S. forests: Documenting variation across forest types, fire severity, and climate regions. *Journal of Geophysical Research*, *117*, G03036. https://doi.org/10.1029/2011JG001935

Giglio, L. (2013). MODIS Collection 5 active fire product User's guide, version 2.5, available at: http://modis-fire.umd.edu/files/MODIS_Fire_Users_Guide_2.5.pdf, last accessed on 1/30/2018.

Giglio, L., Descloitres, J., Justice, C. O., & Kaufman, Y. J. (2003). An enhanced contextual fire detection algorithm for MODIS. *Remote Sensing of Environment*, *87*(2-3), 273–282. https://doi.org/10.1016/S0034-4257(03)00184-6

Hawbaker, T. J., Vanderhoof, M. K., Beal, Y.-J., Takacs, J. D., Schmidt, G. L., Falgout, J. T., et al. (2017). Mapping burned areas using dense time-series of Landsat data. *Remote Sensing of Environment*, *198*, 504–522. https://doi.org/10.1016/j.rse.2017.06.027

Hély, C., Alleaume, S., Swap, R. J., Shugart, H. H., & Justice, C. O. (2003). SAFARI-2000 characterization of fuels, fire behavior, combustion completeness, and emissions from experimental burns in infertile grass savannas in western Zambia. *Journal of Arid Environments*, *54*(2), 381–394. https://doi.org/10.1006/jare.2002.1097

Heward, H., Smith, A. M. S., Roy, D. P., Tinkham, W. T., Hoffman, C. M., Morgan, P., & Lannom, K. O. (2013). Is burn severity related to fire intensity? Observations from landscape scale remote sensing. *International Journal of Wildland Fire*, *22*(7), 910–918. https://doi.org/10.1071/WF12087

Homer, C. G., Dewitz, J. A., Yang, L., Jin, S., Danielson, P., Xian, G., et al. (2015). Completion of the 2011 National Land Cover Database for the Conterminous United States—Representing a decade of land cover change information. *Photogrammetric Engineering and Remote Sensing*, *81*(5), 345–354.

Hudak, A. T., Dickinson, M. B., Bright, B. C., Kremens, R. L., Loudermilk, E. L., O'Brien, J. J., et al. (2016). Measurements relating fire radiative energy density and surface fuel consumption – RxCADRE 2011 and 2012. *International Journal of Wildland Fire*, *25*(1), 25–37. https://doi.org/10.1071/WF14159

Ichoku, C., & Kaufman, Y. J. (2005). A method to derive smoke emission rates from MODIS fire radiative energy measurements. *IEEE Transactions on Geoscience and Remote Sensing*, *43*(11), 2636–2649. https://doi.org/10.1109/TGRS.2005.857328

IPCC (2006). 2006 IPCC guidelines for National Greenhouse Gas Inventories. In H. S. Eggleston, et al. (Eds.), *Prepared by the National Greenhouse gas Inventories Programme* (Chap. 2, pp. 1–59). IGES, Japan.

Ito, A., & Penner, J. E. (2004). Global estimates of biomass burning emissions based on satellite imagery for the year 2000. *Journal of Geophysical Research*, *109*, D14S05. https://doi.org/10.1029/2003JD004423

Kaiser, J. W., Heil, A., Andreae, M. O., Benedetti, A., Chubarova, N., Jones, L., et al. (2012). Biomass burning emissions estimated with a global fire assimilation system based on observed fire radiative power. *Biogeosciences*, *9*(1), 527–554. https://doi.org/10.5194/bg-9-527-2012

Kasischke, E. S., Loboda, T., Giglio, L., French, N. H. F., Hoy, E. E., de Jong, B., & Riano, D. (2011). Quantifying burned area for North American forests: Implications for direct reduction of carbon stocks. *Journal of Geophysical Research*, *116*, G04003. https://doi.org/10.1029/2011JG001707

Kaufman, Y. J., Remer, L., Ottmar, R., Ward, D., Li, R.-R., Kleidman, R., et al. (1996). Relationship between remotely sensed fire intensity and rate of emission of smoke: SCAR-C experiment. In J. Levin (Ed.), *Global Biomass Burning* (pp. 685–696). Cambridge MA: The MIT Press.

Kaufman, Y. J., Justice, C. O., Flynn, L. P., Kendall, J. D., Prins, E. M., Giglio, L., et al. (1998). Potential global fire monitoring from EOS-MODIS. *Journal of Geophysical Research*, *103*(D24), 32,215–32,238. https://doi.org/10.1029/98JD01644

Keeley, J. E. (2009). Fire intensity, fire severity and burn severity: A brief review and suggested usage. *International Journal of Wildland Fire*, *18*(1), 116–126. https://doi.org/10.1071/WF07049

Key, C. H., &Benson, N. C. (2005). Landscape assessment: Remote sensing of severity, the normalized burn ratio, *Rep*., LA1-LA51 pp, Ogden, UT.

Key, C. H., & Benson, N. C. (2006). Landscape assessment (LA), *FIREMON: Fire effects monitoring and inventory system*. *Gen*. *Tech*. *Rep*. *RMRS-GTR-164-CD*, *Fort Collins*, *CO: US Department of Agriculture*, *Forest Service*, Rocky Mountain Research Station.

Konovalov, I. B., Berezin, E. V., Ciais, P., Broquet, G., Beekmann, M., Hadji-Lazaro, J., et al. (2014). Constraining CO2 emissions from open biomass burning by satellite observations of co-emitted species: A method and its application to wildfires in Siberia. *Atmospheric Chemistry and Physics*, *14*(19), 10383–10410. https://doi.org/10.5194/acp-14-10383-2014

Kremens, R. L., Dickinson, M. B., & Bova, A. S. (2012). Radiant flux density, energy density and fuel consumption in mixed-oak forest surface fires. *International Journal of Wildland Fire*, *21*(6), 722–730. https://doi.org/10.1071/WF10143

Kumar, S. S., Roy, D. P., Boschetti, L., & Kremens, R. (2011). Exploiting the power law distribution properties of satellite fire radiative power retrievals: A method to estimate fire radiative energy and biomass burned from sparse satellite observations. *Journal of Geophysical Research*, *116*, D19303. https://doi.org/10.1029/2011JD015676

Lentile, L. B., Holden, Z. A., Smith, A. M. S., Falkowski, M. J., Hudak, A. T., Morgan, P., et al. (2006). Remote sensing techniques to assess active fire characteristics and post-fire effects. *International Journal of Wildland Fire*, *15*(3), 319–345. https://doi.org/10.1071/WF05097

Lentile, L. B., Smith, A. M. S., Hudak, A. T., Morgan, P., Bobbitt, M. J., Lewis, S. A., & Robichaud, P. R. (2009). Remote sensing for prediction of 1-year post-fire ecosystem condition. *International Journal of Wildland Fire*, *18*(5), 594–608. https://doi.org/10.1071/WF07091

Loveland, T. R., Reed, B. C., Brown, J. F., Ohlen, D. O., Zhu, Z., Yang, L., & Merchant, J. W. (2000). Development of a global land cover characteristics database and IGBP DISCover from 1 km AVHRR data. *International Journal of Remote Sensing*, *21*(6-7), 1303–1330. https://doi.org/10.1080/014311600210191

Lutes, D. C., Keane, R. E., & Caratti, J. F. (2009). A surface fuel classification for estimating fire effects. *International Journal of Wildland Fire*, *18*(7), 802–814. https://doi.org/10.1071/WF08062

Lydersen, J. M., Collins, B. M., Ewell, C. M., Reiner, A. L., Fites, J. A., Dow, C. B., et al. (2014). Using field data to assess model predictions of surface and ground fuel consumption by wildfire in coniferous forests of California. *Journal of Geophysical Research: Biogeosciences*, *119*, 223–235. https://doi.org/10.1002/2013JG002475

Mathews, B. J., Strand, E. K., Smith, A. M. S., Hudak, A. T., Hudak, A. T., Dickinson, B., & Kremens, R. L. (2016). Laboratory experiments to estimate interception of infrared radiation by tree canopies. *International Journal of Wildland Fire*, *25*(9), 1009–1014. https://doi.org/10.1071/WF16007

Meigs, G. W., Donato, D. C., Campbell, J. L., Martin, J. G., & Law, B. E. (2009). Forest fire impacts on carbon uptake, storage, and emission: The role of burn severity in the eastern cascades, Oregon. *Ecosystems*, *12*(8), 1246–1267. https://doi.org/10.1007/s10021-009-9285-x

Moody, J. A., Martin, D. A., Haire, S. L., & Kinner, D. A. (2008). Linking runoff response to burn severity after a wildfire. *Hydrological Processes*, *22*(13), 2063–2074. https://doi.org/10.1002/hyp.6806

Ottmar, R. D., Prichard, S. J., Vihnanek, R. E., & Sandberg, D. V. (2006). *Modification and validation of fuel consumption models for shrub and forested lands in the Southwest, Pacific Northwest, Rockies, Midwest, Southeast and Alaska, Joint Fire Science Program*. Seattle Washington.

Ottmar, R. D., Sandberg, D. V., Riccardi, C. L., & Prichard, S. J. (2007). An overview of the Fuel Characteristic Classification System—Quantifying, classifying, and creating fuelbeds for resource planning, This article is one of a selection of papers published in the special forum on the fuel characteristic classification system. *Canadian Journal of Forest Research*, *37*(12), 2383–2393. https://doi.org/10.1139/X07-077

Pellizzaro, G., Cesaraccio, C., Duce, P., Ventura, A., & Zara, P. (2007). Relationships between seasonal patterns of live fuel moisture and meteorological drought indices for Mediterranean shrubland species. *International Journal of Wildland Fire*, *16*(2), 232–241. https://doi.org/10.1071/WF06081

Peterson, D., Wang, J., Ichoku, C., Hyer, E., & Ambrosia, V. (2013). A sub-pixel-based calculation of fire radiative power from MODIS observations: 1: Algorithm development and initial assessment. *Remote Sensing of Environment*, *129*(0), 262–279. https://doi.org/10.1016/j.rse.2012.10.036

Pettinari, M. L., & Chuvieco, E. (2016). Generation of a global fuel data set using the Fuel Characteristic Classification System. *Biogeosciences*, *13*(7), 2061–2076. https://doi.org/10.5194/bg-13-2061-2016

Price, O. F., & Gordon, C. E. (2016). The potential for LiDAR technology to map fire fuel hazard over large areas of Australian forest. *Journal of Environmental Management*, *181*, 663–673. https://doi.org/10.1016/j.jenvman.2016.08.042

Prichard, S. J., Sandberg, D. V., Ottmar, R. D., Eberhardt, E., Andreu, A., Eagle, P., & Swedin, K. (2013). Fuel characteristic classification system version 3.0: Technical documentation Rep., 79 pp, U.S. Department of Agriculture, Forest Service, Pacific Northwest Research Station.

Prichard, S. J., Kennedy, M. C., Wright, C. S., Cronan, J. B., & Ottmar, R. D. (2017). Predicting forest floor and woody fuel consumption from prescribed burns in southern and western pine ecosystems of the United States. *Forest Ecology and Management*, *405*, 328–338. https://doi.org/10.1016/j.foreco.2017.09.025

Prins, E. M., Feltz, J. M., Menzel, W. P., & Ward, D. E. (1998). An overview of GOES-8 diurnal fire and smoke results for SCAR-B and 1995 fire season in South America. *Journal of Geophysical Research*, *103*(D24), 31,821–31,835. https://doi.org/10.1029/98JD01720

Randerson, J. T., Chen, Y., van der Werf, G. R., Rogers, B. M., & Morton, D. C. (2012). Global burned area and biomass burning emissions from small fires. *Journal of Geophysical Research*, *117*, G04012. https://doi.org/10.1029/2012JG002128

Roberts, G. J., & Wooster, M. J. (2008). Fire detection and fire characterization over Africa using Meteosat SEVIRI. *IEEE Transactions on Geoscience and Remote Sensing*, *46*(4), 1200–1218. https://doi.org/10.1109/TGRS.2008.915751

Roberts, G., & Wooster, M. J. (2014). Development of a multi-temporal Kalman filter approach to geostationary active fire detection & fire radiative power (FRP) estimation. *Remote Sensing of Environment*, *152*(0), 392–412. https://doi.org/10.1016/j.rse.2014.06.020

Roberts, G., Wooster, M. J., Perry, G. L. W., Drake, N., Rebelo, L. M., & Dipotso, F. (2005). Retrieval of biomass combustion rates and totals from fire radiative power observations: Application to southern Africa using geostationary SEVIRI imagery. *Journal of Geophysical Research*, *110*, D21111. https://doi.org/10.1029/2005JD006018

Rocha, A. V., & Shaver, G. R. (2011). Burn severity influences postfire CO2 exchange in arctic tundra. *Ecological Applications*, *21*(2), 477–489. https://doi.org/10.1890/10-0255.1

Roy, D. P., & Landmann, T. (2005). Characterizing the surface heterogeneity of fire effects using multi-temporal reflective wavelength data. *International Journal of Remote Sensing*, *26*(19), 4197–4218. https://doi.org/10.1080/01431160500112783

Roy, D. P., Boschetti, L., & Trigg, S. N. (2006). Remote sensing of fire severity: Assessing the performance of the normalized burn ratio. *IEEE Geoscience and Remote Sensing Letters*, *3*(1), 112–116. https://doi.org/10.1109/LGRS.2005.858485

Roy, D. P., Boschetti, L., Maier, S. W., & Smith, A. M. S. (2010). Field estimation of ash and char colour-lightness using a standard grey scale. *International Journal of Wildland Fire*, *19*(6), 698–704. https://doi.org/10.1071/WF09133

Schmidt, C. C., & Prins, E. M. (2003). *GOES wildfire ABBA applications in the western hemisphere*. Paper presented at 2nd International Wildland Fire Ecology and Fire Management Congress and 5th Symp. on Fire and Forest Meteorology, Citeseer.

Seiler, W., & Crutzen, P. (1980). Estimates of gross and net fluxes of carbon between the biosphere and the atmosphere from biomass burning. *Climatic Change*, *2*(3), 207–247. https://doi.org/10.1007/BF00137988

Smith, A. M. S., & Hudak, A. T. (2005). Estimating combustion of large downed woody debris from residual white ash. *International Journal of Wildland Fire*, *14*(3), 245–248. https://doi.org/10.1071/WF05011

Smith, A. M. S., & Wooster, M. J. (2005). Remote classification of head and backfire types from MODIS fire radiative power and smoke plume observations. *International Journal of Wildland Fire*, *14*(3), 249–254. https://doi.org/10.1071/WF05012

Smith, A. M. S., Tinkham, W. T., Roy, D. P., Boschetti, L., Kremens, R. L., Kumar, S. S., et al. (2013). Quantification of fuel moisture effects on biomass consumed derived from fire radiative energy retrievals. *Geophysical Research Letters*, *40*, 6298–6302. https://doi.org/10.1002/2013GL058232

Sofiev, M., Vankevich, R., Lotjonen, M., Prank, M., Petukhov, V., Ermakova, T., et al. (2009). An operational system for the assimilation of the satellite information on wild-land fires for the needs of air quality modelling and forecasting. *Atmospheric Chemistry and Physics*, *9*(18), 6833–6847. https://doi.org/10.5194/acp-9-6833-2009

Sparks, A. M., Boschetti, L., Smith, A. M. S., Tinkham, W. T., Lannom, K. O., & Newingham, B. A. (2015). An accuracy assessment of the MTBS burned area product for shrub–steppe fires in the northern Great Basin, United States. *International Journal of Wildland Fire*, *24*(1), 70–78. https://doi.org/10.1071/WF14131

Steel, Z. L., Safford, H. D., & Viers, J. H. (2015). The fire frequency-severity relationship and the legacy of fire suppression in California forests. *Ecosphere*, *6*(1), art8–ar23. https://doi.org/10.1890/ES14-00224.1

van der Werf, G. R., Randerson, J. T., Giglio, L., Collatz, G. J., Mu, M., Kasibhatla, P. S., et al. (2010). Global fire emissions and the contribution of deforestation, savanna, forest, agricultural, and peat fires (1997–2009). *Atmospheric Chemistry and Physics*, *10*(23), 11,707–11,735. https://doi.org/10.5194/acp-10-11707-2010

van Leeuwen, T. T., van der Werf, G. R., Hoffmann, A. A., Detmers, R. G., Rücker, G., French, N. H. F., et al. (2014). Biomass burning fuel consumption rates: A field measurement database. *Biogeosciences*, *11*(24), 7305–7329. https://doi.org/10.5194/bg-11-7305-2014

Veraverbeke, S., & Hook, S. J. (2013). Evaluating spectral indices and spectral mixture analysis for assessing fire severity, combustion completeness and carbon emissions. *International Journal of Wildland Fire*, *22*(5), 707–720. https://doi.org/10.1071/WF12168

Vermote, E., Ellicott, E., Dubovik, O., Lapyonok, T., Chin, M., Giglio, L., & Roberts, G. J. (2009). An approach to estimate global biomass burning emissions of organic and black carbon from MODIS fire radiative power. *Journal of Geophysical Research*, *114*, D18205. https://doi.org/10.1029/2008JD011188

Waltz, A. E. M., Stoddard, M. T., Kalies, E. L., Springer, J. D., Huffman, D. W., & Meador, A. S. (2014). Effectiveness of fuel reduction treatments: Assessing metrics of forest resiliency and wildfire severity after the Wallow Fire, AZ. *Forest Ecology and Management*, *334*, 43–52. https://doi.org/10.1016/j.foreco.2014.08.026

Ward, D. E., Hao, W. M., Susott, R. A., Babbitt, R. E., Shea, R. W., Kauffman, J. B., & Justice, C. O. (1996). Effect of fuel composition on combustion efficiency and emission factors for African savanna ecosystems. *Journal of Geophysical Research*, *101*(D19), 23,569–23,576. https://doi.org/10.1029/95JD02595

Wickham, J. D., Stehman, S. V., Gass, L., Dewitz, J., Fry, J. A., & Wade, T. G. (2013). Accuracy assessment of NLCD 2006 land cover and impervious surface. *Remote Sensing of Environment*, *130*, 294–304. https://doi.org/10.1016/j.rse.2012.12.001

Wolfe, R. E., Roy, D. P., & Vermote, E. (1998). MODIS land data storage, gridding, and compositing methodology: Level 2 grid. *IEEE Transactions on Geoscience and Remote Sensing*, *36*(4), 1324–1338. https://doi.org/10.1109/36.701082

Wolfe, R. E., Nishihama, M., Fleig, A. J., Kuyper, J. A., Roy, D. P., Storey, J. C., & Patt, F. S. (2002). Achieving sub-pixel geolocation accuracy in support of MODIS land science. *Remote Sensing of Environment*, *83*(1-2), 31–49. https://doi.org/10.1016/S0034-4257(02)00085-8

Wooster, M. J. (2002). Small-scale experimental testing of fire radiative energy for quantifying mass combusted in natural vegetation fires. *Geophysical Research Letters*, *29*(21), 2027. https://doi.org/10.1029/2002GL015487

Wooster, M. J., Zhukov, B., & Oertel, D. (2003). Fire radiative energy for quantitative study of biomass burning: Derivation from the BIRD experimental satellite and comparison to MODIS fire products. *Remote Sensing of Environment*, *86*(1), 83–107. https://doi.org/10.1016/S0034-4257(03)00070-1

Wooster, M. J., Roberts, G., Perry, G. L. W., & Kaufman, Y. J. (2005). Retrieval of biomass combustion rates and totals from fire radiative power observations: FRP derivation and calibration relationships between biomass consumption and fire radiative energy release. *Journal of Geophysical Research*, *110*, D24311. https://doi.org/10.1029/2005JD006318

Xu, W., Wooster, M. J., Roberts, G., & Freeborn, P. (2010). New GOES imager algorithms for cloud and active fire detection and fire radiative power assessment across North, South and Central America. *Remote Sensing of Environment*, *114*(9), 1876–1895. https://doi.org/10.1016/j.rse.2010.03.012

Yokelson, R. J., Burling, I. R., Gilman, J. B., Warneke, C., Stockwell, C. E., de Gouw, J., et al. (2013). Coupling field and laboratory measurements to estimate the emission factors of identified and unidentified trace gases for prescribed fires. *Atmospheric Chemistry and Physics*, *13*(1), 89–116. https://doi.org/10.5194/acp-13-89-2013

Zhang, X., Kondragunta, S., Schmidt, C., & Kogan, F. (2008). Near real time monitoring of biomass burning particulate emissions (PM2.5) across contiguous United States using multiple satellite instruments. *Atmospheric Environment*, *42*(29), 6959–6972. https://doi.org/10.1016/j.atmosenv.2008.04.060

Zhang, X., Kondragunta, S., Ram, J., Schmidt, C., & Huang, H.-C. (2012). Near-real-time global biomass burning emissions product from geostationary satellite constellation. *Journal of Geophysical Research*, *117*, D14201. https://doi.org/10.1029/2012JD017459

Zhang, X., Kondragunta, S., & Roy, D. P. (2014). Interannual variation in biomass burning and fire seasonality derived from geostationary satellite data across the contiguous United States from 1995 to 2011. *Journal of Geophysical Research: Biogeosciences*, *119*, 1147–1162. https://doi.org/10.1002/2013JG002518

Zhang, F., Wang, J., Ichoku, C., Hyer, E. J., Yang, Z., Ge, C., et al. (2014). Sensitivity of mesoscale modeling of smoke direct radiative effect to the emission inventory: A case study in northern sub-Saharan African region. *Environmental Research Letters*, *9*(7), 075002. https://doi.org/10.1088/1748-9326/9/7/075002